Tribology International 91 (2015) 198–205

Contents lists available at ScienceDirect

Tribology International

journal homepage: www.elsevier.com/locate/triboint

Synergism between corrosion and wear on CoCrMo – Al_2O_3 biocomposites in a physiological solution

A.M. Ribeiro [a], A.C. Alves [a], L.A. Rocha [a,b], F.S. Silva [a,c], F. Toptan [a,c,*]

[a] Centre for Mechanics and Materials Technologies (CT2M), Universidade do Minho, Azurém, 4800-058 Guimarães, Portugal
[b] UNESP—Univ. Estadual Paulista, Faculdade de Ciências de Bauru, Dep. Física, 17033-360 Bauru, SP, Brazil
[c] Universidade do Minho, Dept. Eng. Mecânica, Azurém, 4800-058 Guimarães, Portugal

ARTICLE INFO

Article history:
Received 27 August 2014
Received in revised form
23 December 2014
Accepted 19 January 2015
Available online 28 January 2015

Keywords:
Metal matrix composite
Corrosive degradation
Synergism of wear and corrosion
Tribochemistry

ABSTRACT

The use of metal matrix composite structures in biomedical implants can be a solution for decreasing the amount of degradation products. Thus, the present work aims to investigate the synergism between corrosion and wear on CoCrMo matrix 10% (vol) Al_2O_3 particle reinforced composites in phosphate buffer solution (PBS) at body temperature. Corrosion behavior was investigated by electrochemical impedance spectroscopy and potentiodynamic polarization. Tribocorrosion tests were performed under open circuit potential, as well as under cathodic and anodic potentiostatic conditions using a reciprocating ball-on-plate tribometer. Results suggest that the addition of Al_2O_3 particles did not create a significant effect on corrosion behavior of CoCrMo alloy, however, it increased the wear resistance and decreased the corrosion kinetics when sliding in PBS solution.

1. Introduction

CoCrMo alloys are being widely used for load-bearing and articulating orthopedic implants owing to their good balance in strength, fatigue, wear, and corrosion resistance [1–5]. However, as articulating implants are under tribological contact surrounded corrosive body fluids, the material degradation can be enhanced by the simultaneous action of wear and corrosion [6]. Moreover, wear and corrosion products that are generated locally by the implant interfaces may lead to periprosthetic inflammation and implant loosening [7,8]. Besides, released metallic ions from the implant material may cause allergic reactions, osteolysis and implant failure [9].

Al_2O_3 coatings have been considered as a solution to minimize the problems related to wear debris and metallic ion release. It has been reported that $Al_2O_3 - Al_2O_3$ bearing couples can lower the wear rates more than 50 times when compared to the standard CoCr – UHMWPE couples. However, low fracture toughness of ceramics is a major concern since even a slow crack growth under stresses well below their fracture strength may be a risk leading to catastrophic bearing failure in implant materials [7].

It is well known that problems related to the low fracture toughness of the monolithic ceramics can be overcome by using composite structures [10]. During the last decades, metal matrix composites (MMCs) reinforced with hard ceramic phases are being used for various wear resistant applications [11]. Individual wear and corrosion behavior of MMCs have extensively been studied and it is known that improved wear resistance of MMCs is mainly linked to the direct strengthening effect of the particles occurring with the transferring of the load from matrix to the reinforcement, together with indirect strengthening mechanisms that is related to dislocation strengthening, Orowan strengthening and grain size refinement or modification of the matrix alloy with the effect of the reinforcement phase addition [11,12]. However, corrosion studies on MMCs showed that addition of the reinforcement phase may deteriorate the corrosion behavior through a galvanic coupling between the matrix and the reinforcement, selective or localized corrosion at the matrix/reinforcement interface, or chemical degradation of the interphases and the reinforcement [13–22]. The literature on the tribocorrosion behavior of MMCs, on the other hand, is very limited as compared to the ones on the individual wear and corrosion studies. Studies showed that reinforcing metallic materials by hard ceramic particles can also improve the tribocorrosion behavior by the load carrying role of the reinforcement particles resulting in less wear and corrosion damage on the matrix metal [23–25]. However, if the matrix/reinforcement bonding is weak, and the reinforcing particles are not strong enough to withstand the loads, reinforcing particles may be detached or fragmented under the sliding which may result even worse wear behavior as compared to the unreinforced alloy due to the third body effect of the particles [26].

* Corresponding author at: Universidade do Minho, Dept. Eng. Mecânica, Azurém, 4800-058 Guimarães, Portugal. Tel.: +351 253 510 231; fax: +351 253 516 007.
E-mail address: ftoptan@dem.uminho.pt (F. Toptan).

http://dx.doi.org/10.1016/j.triboint.2015.01.018
0301-679X/

Corrosion behavior of CoCrMo alloys have been extensively studied, besides, several reports are available on the tribocorrosion behavior of these alloys [27–33]. However, the literature on the CoCrMo matrix composites for biomedical application is very limited. Grądzka-Dahlke et al. [34] studied the effect of calcium pyrophosphate, boron carbide and silicon nitride additions on the mechanical and tribological properties of CoCrMo and reported that calcium pyrophosphate addition resulted in better properties since the other particles lead to third body wear under sliding. Oksiuta et al. [35] studied the corrosion behavior of bioactive glass reinforced CoCrMo matrix composites and reported that composites exhibited better corrosion properties as compared to the base alloy although ultimate compressing strength and elastic properties of the composites were compromised with increasing amount of the bioglass addition.

A recent study by some of the present authors [22] presented a first insight on the tribocorrosion behavior of CoCrMo – Al_2O_3 composites in 8 g/l NaCl solution at body temperature and reported lower tendency to corrosion under sliding as compared to its base alloy. However, the composite materials did not exhibit an improvement on the wear rate mainly due to the insufficient bonding at the matrix/reinforcement interface. It has been reported that the rough surfaces of the spherical Al_2O_3 reinforcing particles inhibited the efficient physical contact with the matrix resulting on with voids at the interface. In the present work, CoCrMo – Al_2O_3 composites were processed by using angular Al_2O_3 particles having smooth surfaces in order to obtain a better physical contact between the matrix and the reinforcement. By performing the tribocorrosion tests under anodic or cathodic potentiostatic polarization it is possible to evaluate the synergistic effect between corrosion and wear [30]. Therefore, the present study aimed at exploring the synergism between corrosion and wear on CoCrMo – 10Al_2O_3 biocomposite in a phosphate buffered saline (PBS) physiological solution at body temperature.

2. Experimental procedure

2.1. Materials

CoCrMo and its composites reinforced by 10% (vol.) Al_2O_3 were produced by using CoCrMo (Nobilmetal, Nobil 4000, Villafranca d'Asti, Italy) and Al_2O_3 (Bego, Germany) particles in spherical and angular shapes, respectively. The chemical composition of the CoCrMo particles is given in Table 1 and the particle size distributions (obtained by a laser particle analyzer, Malvern Series 2600) are given in Table 2.

2.2. Processing

Homogenous CoCrMo – Al_2O_3 powder mixtures were obtained by using a ball mill rotating at 80 rpm for 3 h. Before processing, the powder mixtures were dried in a muffle furnace at 105 °C for 1 h in order to remove the humidity. The samples were produced by hot pressing at 1000 °C under 0.01 mbar of vacuum and a constant pressure of 40 MPa with a sintering time of 30 min. The details of the processing procedure is given elsewhere [33].

Prior to testing and characterization, the samples were ground down to 4000 mesh size SiC paper followed by polishing with diamond paste down to 1 μm. Finally, the samples were ultrasonically cleaned for 10 min in propanol followed by rinsing in distilled water for 5 min. In order to obtain the similar surface conditions, each sample was kept in a desiccator for 24 h before starting the tests.

Table 1
Chemical composition of the CoCrMo alloy (wt%).

Co	Cr	Mo	Si	Mn	Fe	W
62.0	31.0	4.0	2.2	< 1.0	< 1.0	< 1.0

Table 2
Particle size distribution.

Particle size distribution (μm)	*D* [v, 0.1]	*D* [v, 0.5]	*D* [v, 0.9]
CoCrMo	5.38	9.61	17.16
Al_2O_3	50.87	77.91	120.69

2.3. Corrosion tests

Corrosion tests consisting in electrochemical impedance spectroscopy (EIS) and potentiodynamic polarization (PD) were performed as a sequence in phosphate buffer saline solution (PBS; 0.2 g/l KCl, 0.24 g/l KH_2PO_4, 8 g/l NaCl, 1.44 g/l Na_2HPO_4) at body temperature (37 ± 2 °C) using Gamry Potentiostat/Galvanostat (model Reference – 600). Prior to each test, the pH of the PBS solution was measured using a pH-meter (EUTECH Instruments pH 510) and adjusted to 7.4 ± 0.02 by HCl addition. A conventional three-electrode electrochemical cell (adapted from ASTM: G3-89) with an electrolyte volume of 180 ml was used where a saturated calomel electrode (SCE) was used as the reference electrode, a Pt electrode was used as the counter electrode, and the samples having an exposed area of 0.38 cm^2 was used as the working electrode.

EIS measurements were performed after 120 min of stabilization time at open circuit potential (OCP). EIS data acquisition was performed by scanning a range of frequencies from 63 kHz till 10 mHz with 10 points per frequency decade and the amplitude of the sinusoidal signal was chosen as 10 mV in order to guarantee linearity of the electrode response. Following EIS, PD measurements were performed after a delay time of 10 min at OCP. The polarization scan was performed in anodic direction starting at 0.25 V below the corrosion potential (E_{OCP}) to 1 V with a scanning rate of 0.5 mV/s.

2.4. Tribocorrosion tests

Tribocorrosion tests were performed in an electrochemical cell installed on a ball-on-plate tribometer (CETR-UMT-2) with the working surface of the samples having 0.79 cm^2 exposed area facing upwards, against the counter-material (10 mm of diameter alumina ball, Ceratec). The tests were carried out at body temperature using the same three-electrode set-up, together with the same potentiostat and 30 ml of the same electrolyte (PBS) that used in corrosion tests. The tests were performed under OCP, as well as under cathodic (−0.9 V vs. SCE) and anodic (+0.25 V vs. SCE) potentiostatic conditions in order to investigate the synergism between corrosion and wear. After stabilization, sliding was started in a reciprocating movement with a total stroke length of 3 mm, frequency of 1 Hz, normal load of 15 N (corresponds to 1.47 GPa maximum Hertzian contact pressure for the unreinforced alloy) and total sliding time of 3 h.

2.5. Characterization

As-processed microstructures were examined by using Leica DM2500 optical microscope (OM) and FEI Nova 200 field emission gun scanning electron microscope (FEG-SEM), equipped with EDAX energy dispersive X-ray spectroscopy (EDS). Porosity values were determined by image analysis technique using Leica DM2500 OM and Image J 1.37v image analysis software. Vickers macrohardness values were determined by using Officine Galileo Mod. D 200 tester by a mean of 5 indentations per sample with 30 kg load and 20 s dwelling time.

After corrosion and tribocorrosion tests, the samples were cleaned with the same procedure applied after metallographic sample preparation and the surfaces were characterized by using FEG-SEM/EDS. Besides, the width and the deepness of the wear tracks were measured by a contact profilometer (Mitutoyo Surtest SJ-500) and the wear volumes were calculated following the procedure given elsewhere [33].

3. Results and discussion

3.1. Microstructure and physical properties

Microstructural and structural analysis of the hot pressed CoCrMo alloy was presented elsewhere indicating γ (fcc) phase as the matrix phase of the alloy and CrCo-σ phase as the secondary phase [22]. Fig. 1 presents the OM images taken from the composite exhibiting a relatively homogenous particle distribution that is essential to achieve the desired properties on MMCs [36,37]. Higher magnification OM image is also presented in Fig. 1 showing good physical contact between the matrix and the reinforcement that contributed in obtaining very similar porosity values on the unreinforced alloy ($0.09 \pm 0.06\%$) and the composite ($0.10 \pm 0.01\%$). On the other hand, introduction of alumina particles resulted with an increase on the hardness (420 ± 4 HV_{30}) as compared to the unreinforced alloy (394 ± 12 HV_{30}).

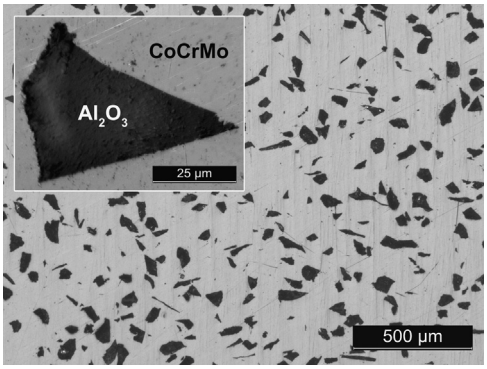

Fig. 1. OM images of CoCrMo – $10Al_2O_3$ composite.

3.2. Corrosion behavior

Experimental and fitted EIS results from CoCrMo and CoCrMo – $10Al_2O_3$ samples are presented in Fig. 2 in the form of Nyquist and Bode diagrams. The Nyquist diagram represents the real and imaginary part of the impedance as a function of the applied frequency perturbation. By comparing the diameters of semi-circles in the Nyquist diagram it is possible to evaluate the corrosion properties of the samples [38]. As general, both materials presented similar behavior, however, slightly higher capacitive behavior of a compact oxide film was observed on the unreinforced alloy since the phase angle was closer to 90° at low and middle frequency range that may be explained by the larger metallic area on the surface.

Fig. 3 presents the equivalent circuit that used on Gamry Echem Analyst software, version 5.61, to fit the experimental data. The quality of fitting was evaluated through their goodness of fitting values and the proposed model describe an adequate behavior of both groups in contact with PBS presenting a goodness of fitting bellow 10^{-3}. The equivalent circuit contains electrolyte resistance (R_e), native oxide film resistance (R_{ox}), and constant phase element (CPE, Q_{ox}), accounting for the non-ideal capacitance of the native oxide film (Fig. 3). This equivalent circuit was also used for CoCrMo – $10Al_2O_3$ that considers a native oxide film formed on the metallic surface of the samples exposed to PBS solution without any discontinuity on matrix/reinforcement interface. Table 3 presents the parameters of fitting results. No significant differences were observed on Q_{ox} and R_{ox} values suggesting similar corrosion resistance on the unreinforced alloy and the composite samples.

Fig. 4 presents representative potentiodynamic polarization curves and Table 4 presents the values of corrosion potential ($E_{(i=0)}$), corrosion current density (i_{corr}) obtained by Tafel extrapolation method, together with passivation current density (i_{pass}). Through the polarization curves it can be seen that the alloy and the composite exhibited similar polarization behavior. In the anodic domain, both materials presented a passivation plateau due to the formation of the passive oxide film as it has already been reported for hot pressed CoCrMo alloy [22,33,39].

Fig. 5 presents backscattered electron (BSE) images of the hot pressed alloy and the composite after the corrosion tests. Homogenous dissolution of γ matrix phase was observed on all samples whereas σ phase appears not to be significantly affected by corrosion. Besides, good physical contact between matrix and the reinforcement was not affected by the corrosion tests on the composite samples.

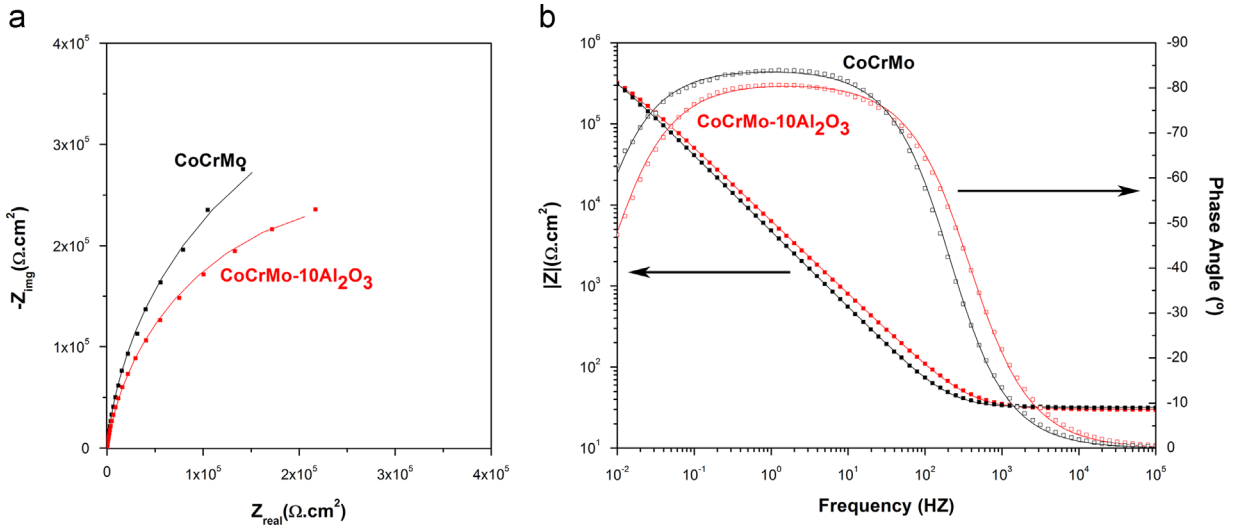

Fig. 2. a) Nyquist and b) Bode diagrams of experimental data and fitted curves.

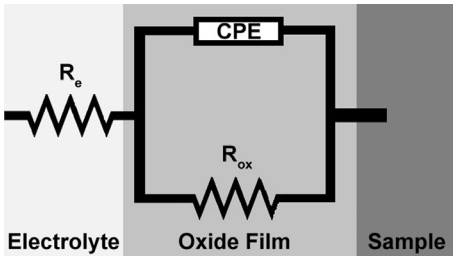

Fig. 3. Equivalent circuit used for CoCrMo and CoCrMo – $10Al_2O_3$ samples.

Table 3
Equivalent circuit parameters obtained from EIS data.

Samples	Q_{ox} ($\times 10^{-5}$ s^n Ω^{-1} cm^{-2})	R_{ox} ($\times 10^6$ Ω cm^2)
CoCrMo	3.08 ± 0.60	0.66 ± 0.20
CoCrMo – $10Al_2O_3$	2.89 ± 0.16	0.68 ± 0.26

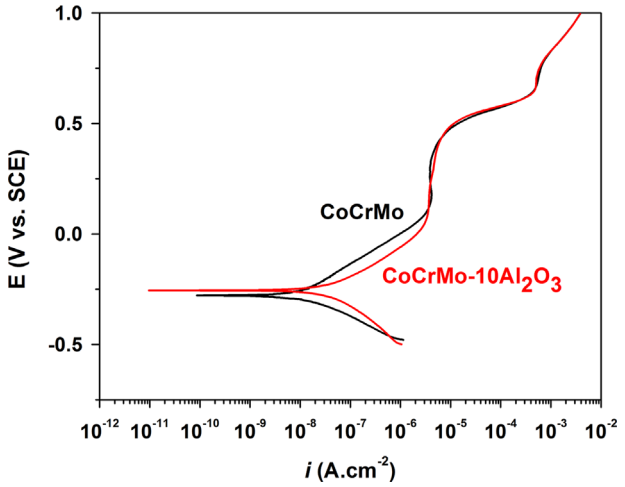

Fig. 4. Representative potentiodynamic polarization curves for CoCrMo and CoCrMo – $10Al_2O_3$ samples in PBS.

Table 4
Corrosion potential ($E_{(i=0)}$), corrosion current density (i_{corr}) and passivation current density (i_{pass})values.

Samples	$E_{(i=0)}$ (V)	i_{corr} ($\times 10^{-6}$ A cm^{-2})	i_{pass} ($\times$ 10^{-6} A cm^{-2})
CoCrMo	-0.29 ± 0.04	336 ± 175	4.34 ± 0.25
CoCrMo – $10Al_2O_3$	-0.22 ± 0.03	546 ± 141	3.82 ± 0.13

3.3. Tribocorrosion behavior

3.3.1. Triboelectrochemical analysis

The evolution of OCP and current density under anodic potentiostatic conditions for CoCrMo and CoCrMo – $10Al_2O_3$ samples recorded before, during and after sliding in PBS solution presented in Fig. 6, together with COF values are recorded during sliding. Before sliding, both OCP and current density values were stable for both materials due to the presence of a passive oxide film on the surface in contact with the electrolyte. When sliding started, a sudden decrease on the OCP (Fig. 6a) and a sudden increase on the current density (Fig. 6b) were recorded for both materials due to the mechanical damage of the passive film, leading to the formation of active sites on the worn area. Thus, under sliding, thermodynamic tendency for corrosion and corrosion kinetics were increased on both samples [22,30,31,33].

When the evolution of OCP is considered (Fig. 6a), it can be seen that the unreinforced alloy presented a smaller drop on the potential on the onset of the sliding as compared to the composite. During the sliding, the unreinforced alloy presented relatively stable average OCP values but larger oscillations. The composite presented smoother evolution but gradually increased values that reached near the ones of the unreinforced alloy at the end of the sliding. On the other hand, both group of samples presented similar average COF values during the sliding, however the evolution was smoother on the composite.

The evolution of current density under sliding (Fig. 6b) presented different trends that were observed on the evolution of OCP. Under sliding, the unreinforced alloy presented higher current densities indicating elevated corrosion kinetics. Besides, waves were observed on the current density evolution for both groups of samples during the sliding. COF values of the composite under anodic potentiostatic conditions presented very similar behavior compared to the ones obtained under OCP, however, the values obtained on the unreinforced alloy presented smoother, but gradually increased values as compared to the OCP conditions and the values were always higher than the ones obtained from the composite.

When sliding stopped, the OCP values increased and the current density values decreased near to the initial values recorded before sliding due to the recovery of the passive oxide film [22,30,31,33].

3.3.2. Total material loss

Fig. 7a presents the wear track profiles for CoCrMo and CoCrMo – $10Al_2O_3$ samples, under cathodic potentiostatic conditions (CP), OCP and anodic potentiostatic conditions (AP), taken from the centre of the wear tracks. It can be seen on the wear profiles that in all conditions, CoCrMo samples presented smoother but deeper wear tracks while composites presented relatively rougher tracks attributed to the protruded Al_2O_3 reinforcing particles. Total wear volume loss values for both materials in all conditions are given in Fig. 7b. As a result of the load carrying effect of the reinforcing particles, composite samples presented lower wear loss values in all conditions. Even so, relatively larger standard deviation values were obtained for all conditions.

If a cathodic potential is applied during sliding, the wear volume represents the material loss due to the mechanical action since the oxidation reaction is not significant [30]. In this condition, a significant decrease in wear volume loss was observed as compared to the other conditions. On the other hand, under anodic polarization where corrosion and wear effects was combined, the wear volume loss presented more than double values as compared to that of the OCP conditions.

3.3.3. Tribocorrosion mechanism

Fig. 8a – f presents representative SEM images of the worn surfaces taken as parallel to the sliding direction for both materials under CP, OCP and AP conditions. Sliding grooves were observed on all samples after all testing conditions (though the surfaces were smoother on the unreinforced samples) indicating abrasive wear that can be occurred due to the penetration of the asperities on the counter material or due to the third body abrasive wear effect given by the loose wear products. Besides, considerable amount of compacted wear debris were observed on the edges of the wear tracks on the unreinforced alloy tested under OCP and AP conditions (Fig. 8b and c). Higher magnification SEM images (Fig. 8g and h) taken from these compacted oxidized debris revealed different morphology but similar chemical composition (Fig. 8i). The debris after OCP conditions presented finer structure whereas debris formed on AP conditions presented flake-like morphology. The flake-like debris formation can be explained by the repeated action

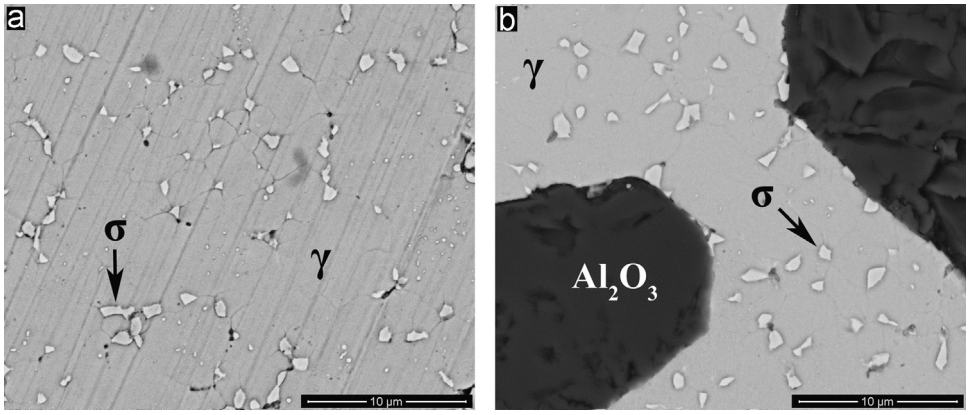

Fig. 5. SEM images of a) CoCrMo and b) CoCrMo – $10Al_2O_3$ samples after the corrosion tests.

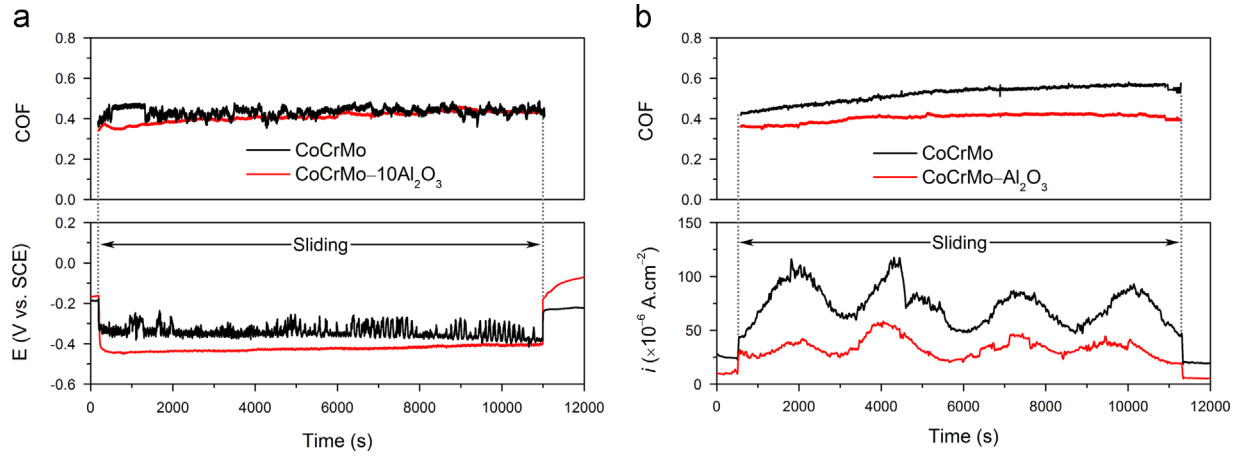

Fig. 6. Evolution of a) OCP and b) current density before, during and after sliding, together with evolution of COF during sliding.

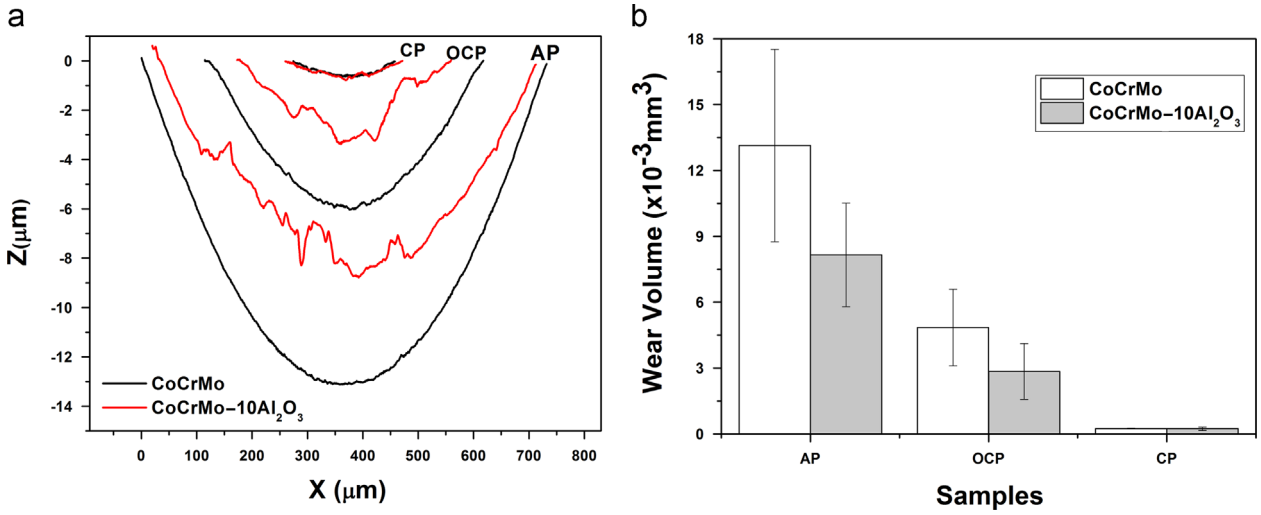

Fig. 7. a) Representative wear track profiles and b) total wear volume loss for each sample and testing condition.

of thickening and breaking of the oxide layer under the influence of the applied anodic potential. This repeated action may also explain the waves observed on the evolution of the current density under sliding (Fig. 6b). Since the corresponding composite sample presented less wear loss due to the load-carrying effect of the reinforcing particles, and also having less metallic area due to the incorporation of reinforcing particles, that repeated action took place in a limited extend thus the waves on the current density evolution recorded were smoother.

Microstructural and profilometric analyses of the worn surfaces revealed that oxidizing conditions during sliding significantly accelerated the tribocorrosion process, and therefore, increased the material loss by the accelerated oxidation of the alloy and repeatedly breaking of the oxide layer by the mechanical action. Besides, relatively thick flake-like oxidized wear debris can also create a third body effect, or in other words, can act as an extra abrasive that can also contribute to the elevated material loss. These results are also in agreement with the study Arenas et al. [30] where the

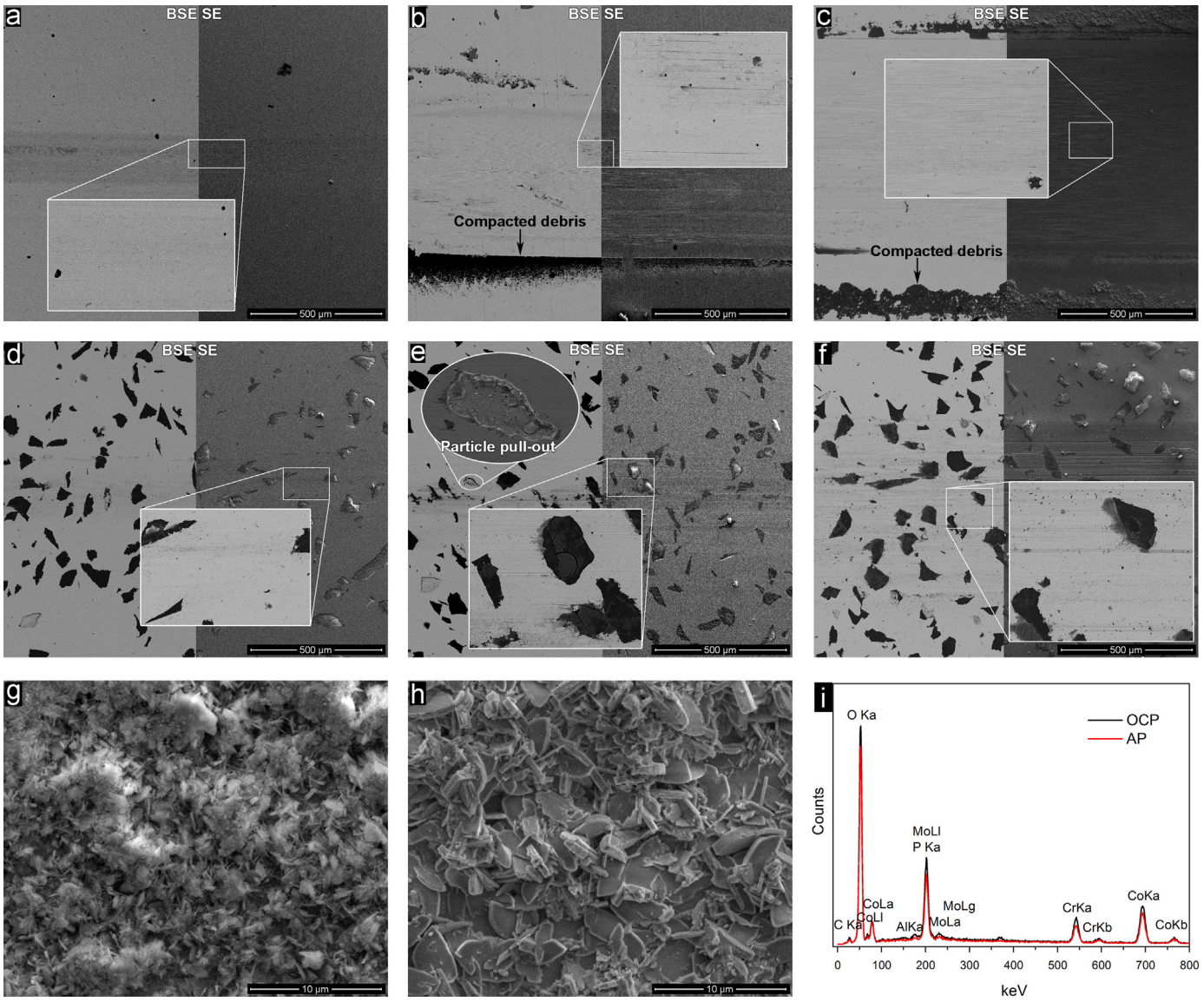

Fig. 8. SEM images of worn a, b, c) CoCrMo and d, e, f) CoCrMo – $10Al_2O_3$ tested under CP, OCP, and AP conditions, respectively; secondary electron (SE) images of wear debris taken from CoCrMo tested under g) OCP and h) AP conditions, and i) the EDS analysis taken from the compacted wear debris.

synergistic effect of corrosion and wear for a CoCrMo alloy was investigated.

The previous work of some of the present authors [33] reported the wear mechanism of the hot pressed CoCrMo alloy mainly as a combination of abrasive and adhesive wear after dry sliding wear and tribocorrosion in 8 g/l NaCl solution. Similar wear mechanism was also observed in the present work for the unreinforced alloy after all testing conditions where abrasive wear that can be characterized by the sliding grooves on the wear track (Fig. 8a – c) and adhesive wear that can be characterized by the material transfer from the samples to the counter material, as can be seen on the SEM images and EDS spectra taken from the worn counter material (alumina ball) surface (Fig. 9. a – c). Sliding grooves were also observed for the composites after all testing conditions (Fig. 8d – f). Additionally, pulling-out of some loosely attached reinforcing particles (Fig. 8e) in the early sliding stage can also cause grooves on the composite samples due to the additional abrasive action. This additional abrasive action given by the pulled-out particles can result in additional damage on the passive film, thus resulting in lower OCP values. However, as sliding proceeded, these entrapped particles may gradually be rejected from the sliding surface resulting in the gradual increase on the potential values for the composites (Fig. 6a). On the other hand, with the absence of the load carrying reinforcing particles, the whole surface of the unreinforced alloy was in contact with the counter material that may create more oxidized wear debris (Fig. 8b and c). If the oxidized wear debris are compacted on the surface, they may act as a protective layer. As contrary, if they are not compacted, they may act as third body particles that can lead to more damage on the surface [24,33,40]. Thus, the larger oscillations on the evolution of OCP for the unreinforced alloy may be attributed to the repeated compaction removing of the wear debris during sliding (Fig. 6a).

On the other hand, wear damage and material transfer from samples to the ball under CP and OCP conditions were considerably less on the composites samples as compared to the unreinforced alloy (Fig. 9. d – f) that may be considered as another consequence of the load carrying effect of the reinforcing particles. Nevertheless, under AP conditions, both counter surfaces exhibited similar EDS spectra that may be explained by the thickened oxide layer by the applied potential that got in contact and broken by the counter material, repeatedly.

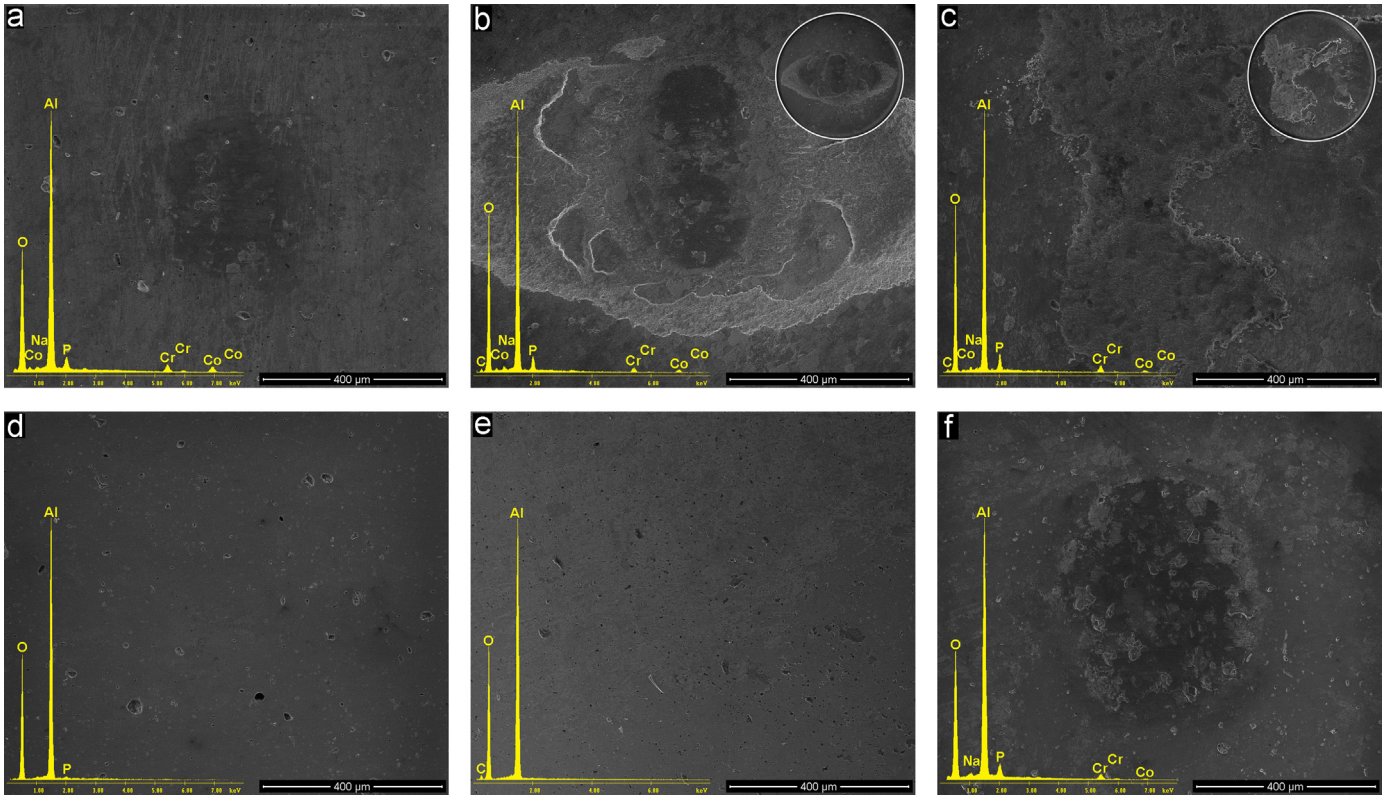

Fig. 9. Low vacuum SEM images of worn counter material (alumina ball) surfaces corresponding to a, b, c) CoCrMo and d, e, f) CoCrMo – 10Al2O3 tested under CP, OCP, and AP conditions, respectively, together with the EDS spectra taken from the wear scars (lower magnification images showing entire wear scar are also given in b and c).

4. Conclusions

Within the framework of this study, the followings can be concluded:

1) The addition of Al_2O_3 particle did not create a significant effect on corrosion behavior of CoCrMo alloy.
2) CoCrMo – 10Al_2O_3 composites presented lower wear volume loss due to the increased wear resistance providing by ceramic particles.
3) The wear volume loss under AP was more than double as compared to OCP condition indicating that the oxidizing conditions greatly accelerated the tribocorrosion process.

Acknowledgments

This study was supported by the Portuguese Foundation for Science and Technology (FCT–Portugal), under the project EXCL/EMS-TEC/0460/2012, and The Calouste Gulbenkian Foundation through “Programa de Mobilidade Académica para Professores”. The authors also would like to thank Prof. Amílcar Ramalho (Universidade de Coimbra) for the provision of profilometry facilities.

References

[1] Yen SK, Hsu SW. Electrolytic Al2O3 coating on Co–Cr–Mo implant alloys of hip prosthesis. J Biomed Mater Res 2001;54:412–8.
[2] Bae IJ, Standard OC, Roger GJ, Brazil D. Phase and microstructural development in alumina sol–gel coatings on CoCr alloy. J Mater Sci Mater Med 2004;15:959–66.
[3] Casabán Julián L, Igual Muñoz A. Influence of microstructure of HC CoCrMo biomedical alloys on the corrosion and wear behaviour in simulated body fluids. Tribol Int 2011;44:318–29.
[4] Contu F, Elsener B, Böhni H. Corrosion behaviour of CoCrMo implant alloy during fretting in bovine serum. Corros Sci 2005;47:1863–75.
[5] Vamsi Krishna B, Xue W, Bose S, Bandyopadhyay A. Functionally graded Co–Cr–Mo coating on Ti–6Al–4V alloy structures. Acta Biomater 2008;4:697–706.
[6] Thomann UI, Uggowitzer PJ. Wear–corrosion behavior of biocompatible austenitic stainless steels. Wear 2000;239:48–58.
[7] Rahaman MN, Yao A, Bal BS, Garino JP, Ries MD. Ceramics for prosthetic hip and knee joint replacement. J Am Ceram Soc 2007;90:1965–88.
[8] Caicedo MS, Desai R, McAllister K, Reddy A, Jacobs JJ, Hallab NJ. Soluble and particulate Co–Cr–Mo alloy implant metals activate the inflammasome danger signaling pathway in human macrophages: a novel mechanism for implant debris reactivity. J Orthop Res 2009;27:847–54.
[9] Díaz C, García JA, Mändl S, Rodríguez RJ. Plasma immersion ion implantation for the prevention of metal ion release from CoCrMo alloys. IEEE Trans Plasma Sci 2011;39:3045–8.
[10] Rosso M. Ceramic and metal matrix composites: routes and properties. J Mater Process Technol 2006;175:364–75.
[11] Russell AM, Lee KL. Structure property relations in nonferrous metals. New Jersey: John Wiley & Sons, Inc; 2005.
[12] Chawla N, Shen Y-L. Mechanical behavior of particle reinforced metal matrix composites. Adv Eng Mater 2001;3:357–70.
[13] Shreir L. 3rd ed.Corrosion, 1. . London: Butterworth-Heinemann; 1994.
[14] Winkler SL, Flower HM. Stress corrosion cracking of cast 7XXX aluminium fibre reinforced composites. Corros Sci 2004;46:903–15.
[15] Bobic B, Mitrovic S, Babic M, Bobic I. Corrosion of Aluminium and zinc-aluminium alloys based metal–matrix composites. Tribol Int 2009;31:44–53.
[16] Otani T, McEnaney B, Scott VD. Corrosion of metal matrix composites. In: Fishman SG, Dhingra AK, editors. Cast Reinforced Metal Composites. Metals Park, Ohio: ASM International; 1988. p. 383–90.
[17] Hihara LH, Latanision RM. Corrosion of metal matrix composites. Int Mater Rev 1994;39:245–64.
[18] Yue TM, Wu YX, Man HC. Improvement in the corrosion resistance of aluminum 2009/SiC w composite by Nd/YAG laser surface treatment. J Mater Sci Lett 1999;18:173–5.
[19] Hu J, Chu WY, Fei WD, Zhao LC. Effect of interfacial reaction on corrosion behavior of alumina borate whisker reinforced 6061Al composite. Mater Sci Eng A 2004;374:153–9.
[20] Pardo A, Merino MC, Merino S, Viejo F, Carboneras M, Arrabal R. Influence of reinforcement proportion and matrix composition on pitting corrosion behaviour of cast aluminium matrix composites (A3xx.x/SiCp). Corros Sci 2005;47:1750–64.
[21] Pardo A, Merino MC, Rams J, Merino S, Viejo F, Campo M. Effect of reinforcement coating on the oxidation behavior of AA6061/SiC/20p composite. Oxid Met 2005;63:215–27.

[22] Doni Z, Alves AC, Toptan F, Pinto AM, Rocha LA, Buciumeanu M, et al. Tribocorrosion behaviour of hot pressed CoCrMo – Al_2O_3 composites for biomedical applications. Tribol – Mater Surf Interfaces 2014;8:201–8.
[23] Fang C, Huang CC, Chuang TH. Synergistic effects of wear and corrosion for Al_2O_3 particulate-reinforced 6061 aluminum matrix composites. Metall Mater Trans A 1999;30A:643–51.
[24] Toptan F, Alves AC, Kerti I, Ariza E, Rocha LA. Corrosion and tribocorrosion behaviour of Al-Si-Cu-Mg alloy and its composites reinforced with B4C particles in 0.05 M NaCl solution. Wear 2013;306:27–35.
[25] Benea L. Electrodeposition and tribocorrosion behaviour of ZrO_2–Ni composite coatings. J Appl Electrochem 2009;36:1671–81.
[26] Velhinho A, Botas JD, Ariza E, Gomes JR, Rocha LA. Tribocorrosion studies in centrifugally cast Al-matrix SiC p-reinforced functionally graded composites. Mater Sci Forum 2004;455–456:871–5.
[27] Igual Muñoz A, Casabán Julián L. Influence of electrochemical potential on the tribocorrosion behaviour of high carbon CoCrMo biomedical alloy in simulated body fluids by electrochemical impedance spectroscopy. Electrochim Acta 2010;55:5428–39.
[28] Mathew MT, Runa MJ, Laurent M, Jacobs JJ, Rocha LA, Wimmer MA. Tribocorrosion behavior of CoCrMo alloy for hip prosthesis as a function of loads: a comparison between two testing systems. Wear 2011;271:1210–9.
[29] Yan Y, Neville A, Dowson D, Williams S. Tribocorrosion in implants—assessing high carbon and low carbon Co–Cr–Mo alloys by in situ electrochemical measurements. Tribol Int 2006;39:1509–17.
[30] Arenas MA, Conde A, Damborenea JJ. The role of mechanically activated area on tribocorrosion of CoCrMo. Metall Mater Trans A 2013;44:4382–90.
[31] Figueiredo-Pina CG, Neves AAM, Neves BMB das. Corrosion-wear evaluation of a UHMWPE/Co–Cr couple in sliding contact under relatively low contact stress in physiological saline solution. Wear 2011;271:665–70.
[32] Sinnett-Jones PE, Wharton JA, Wood RJK. Micro-abrasion–corrosion of a CoCrMo alloy in simulated artificial hip joint environments. Wear 2005;259:898–909.
[33] Doni Z, Alves AC, Toptan F, Gomes JR, Ramalho A, Buciumeanu M, et al. Dry sliding and tribocorrosion behaviour of hot pressed CoCrMo biomedical alloy as compared with the cast CoCrMo and Ti6Al4V alloys. Mater Des 2013;52:47–57.
[34] Grądzka-Dahlke M, Dąbrowski JR, Dąbrowski B. Modification of mechanical properties of sintered implant materials on the base of Co–Cr–Mo alloy. J Mater Process Technol 2008;204:199–205.
[35] Oksiuta Z, Dabrowski JR, Olszyna A. Co–Cr–Mo-based composite reinforced with bioactive glass. J Mater Process Technol 2009;209:978–85.
[36] Segurado J, González C, LLorca J. A numerical investigation of the effect of particle clustering on the mechanical properties of composites. Acta Mater 2003;51:2355–69.
[37] Toptan F, Kerti I, Rocha LA. Reciprocal dry sliding wear behaviour of B4Cp reinforced aluminium alloy matrix composites. Wear 2012;290–291:74–85.
[38] Lin CH, Duh JG. Electrochemical impedance spectroscopy (EIS) study on corrosion performance of CrAlSiN coated steels in 3.5wt% NaCl solution. Surf Coat Technol 2009;204:784–7.
[39] Henriques B, Soares D, Silva FS. Microstructure, hardness, corrosion resistance and porcelain shear bond strength comparison between cast and hot pressed CoCrMo alloy for metal-ceramic dental restorations. J Mech Behav Biomed Mater 2012;12:83–92.
[40] Landolt D, Mischler S, Stemp M, Barril S. Third body effects and material fluxes in tribocorrosion systems involving a sliding contact. Wear 2004;256:517–24.